Testing a Cumulus Parameterization With a Cumulus Ensemble Model in Weak Temperature Gradient Mode

David J. Raymond*
New Mexico Tech, Socorro, NM, USA

March 2, 2007

Summary

This paper prototypes a method for calibrating a cumulus parameterization against a cumulus ensemble model. The key to this technique is to run the cumulus model and the parameterization in identical "test cells" which provide forcing typical of that seen over tropical oceans. In particular, the mean temperature profile is relaxed to a reference profile which is assumed to be characteristic of the environment of the convection. This is done by calculating the mean vertical velocity needed to balance heating due to convection, latent heat release, and radiation with adiabatic cooling. This "weak temperature gradient" (WTG) vertical velocity profile is then used to advect moisture vertically and, via mass continuity, through the sides of the test cell, entraining reference profile air as needed.

As an example, a toy cumulus parameterization used previously is altered to reproduce the dependence of rainfall rate on surface wind speed shown by the cumulus ensemble model. This alteration greatly modifies the behavior of simulated large-scale disturbances in an aquaplanet equatorial beta-plane model. In particular, increasing the slope of the rainfall rate-wind speed curve results in the development of much more synoptic-scale variance.

1 Introduction

Ample evidence exists that the form and distribution of tropical convection and precipitation in atmospheric global circulation models (AGCMs) depends strongly on the parametric treatment of deep convection in the models (Slingo et al. 1994; Wang and Schlesinger 1999; Maloney and Hartmann 2001; Randall et al. 2003; Mapes et al. 2004; Zhang and Mu 2005; Zhang et al. 2006). Unfortunately, it is not easy to test incisively whether convection and

* *Corresponding author address:* David J. Raymond, Physics Department and Geophysical Research Center, New Mexico Tech, 801 Leroy Place, Socorro, NM 87801 USA. *Email:* raymond@kestrel.nmt.edu.

other diabatic parameterizations are doing the right thing. The most obvious test is to compare model climatology with observations, but where disagreements are found, they are notoriously difficult to attribute to the actual source of the error.

Frustration with this state of affairs has led to attempts to install separate cumulus ensemble models in each grid box of a global model, each of which carries out the duties of a cumulus parameterization in its assigned box. This so-called superparameterization technique was pioneered by Grabowski and Smolarkiewicz (1999), Grabowski (2001), Khairoutdinov and Randall (2001), and Randall et al. (2003). The hope is that explicit calculation of deep convection over a small sub-region of each grid cell will yield representative statistics for sub-grid fluxes and precipitation which can be applied to the entire cell. In spite of the fact that parametric representations of cloud physics and small clouds must still be provided, these calculations appear promising.

Given the enormous computational cost of such calculations, it seems reasonable to ask whether the additional skill provided by this technique can be accessed in a more economical fashion. In particular, if a cumulus parameterization can be made to mimic quantitatively the behavior of convection in a cumulus ensemble model, then perhaps the calibrated parameterization can be used in place of the ensemble model in each grid cell of the large-scale simulation.

The key to comparing the two is to place the cumulus ensemble model and the candidate parameterization in identical "test cells" which exhibit the approximate range of behaviors actually seen in the grid cells of a large-scale model. A test performed by Sobel and Bretherton (2000) is very enlightening in this regard. Starting from the well-known tendency of the tropical atmosphere to redistribute buoyancy anomalies so as to homogenize the virtual temperature on isobaric surfaces, these investigators decoupled neighboring grid columns from each other in a large-scale model and replaced the complex interaction between columns with the instantaneous relaxation of the temperature profile in each column to a common reference profile. This relaxation was effected by imposing a vertical velocity profile which produced just enough adiabatic cooling to counter the heating produced by the convective parameterization. The vertical velocity computed in this manner was also used to produce a vertical advective tendency in the mixing ratio. Remarkably, the resulting patterns of precipitation and divergence were approximately the same as those which occurred in the full model. Bretherton dubbed this approximation the weak temperature gradient (WTG) approximation (Sobel, Nilsson, and Polvani 2001), and Sobel and Bretherton (2000) showed that the WTG approximation represents reasonably well the net effect on any tropical grid column of the rest of the model.

The success of the WTG approximation tells us how to design our test cell for cumulus parameterizations; calculate the cell-mean vertical velocity profile needed to counter horizontally averaged heating and allow it to advect moisture vertically and entrain air from fixed reference conditions. Raymond and Zeng (2005) implemented just such a test cell for a cumulus ensemble model and Derbyshire et al. (2004) developed a somewhat similar scheme. These ideas have also been explored by Bergman and Sardeshmukh (2004) and Mapes (2004).

Note that this scheme differs somewhat from the more commonly used form of cumulus ensemble model in which the vertical velocity profile responsible for the advective tendencies is derived from observations or other external considerations (Randall et al. 1996; Xu and Randall 1996; Grabowski et al. 1996). Though technically there is nothing wrong with this

approach, it has conceptual problems having to do with the direction of causality if, as we believe is generally true in the tropics, the convection and radiation themselves largely determine the mean vertical velocity (see Raymond and Zeng 2005). The WTG scheme thus differs from the case in which the domain-averaged vertical motion is prescribed in that the mean vertical velocity is determined internally from the condition that the mean virtual temperature profile must continue to approximate that of the surroundings.

The purpose of this paper is to show by example that the procedure outlined above can be carried out. The results should be viewed as a "proof on concept" rather than a definitive result, as more stringent comparisons need to be made between the parameterizations and the model, and the cumulus ensemble model itself needs upgrading in a number of ways. Nevertheless, the model results do highlight the importance of the relationships between surface wind speed, tropospheric humidity, and precipitation and the resulting statistical character of tropical synoptic and intraseasonal disturbances.

In section 2 we describe the WTG approximation test cell and present the cumulus ensemble model calculations needed to calibrate the cumulus parameterization. We modify the cumulus parameterization of Raymond and Torres (1998) and Raymond (2000a, 2001) to match the cumulus ensemble model results in section 3, while in section 4 we explore the effects of these modifications on the power spectra of modeled synoptic and intraseasonal disturbances over tropical oceans. Results are summarized and conclusions are drawn in section 5.

2 The cumulus ensemble model in WTG mode

The WTG test cell is first described in this section, followed by a presentation of results from cumulus ensemble model calculations.

2.1 The WTG test cell

Raymond and Zeng (2005) describe the use of WTG in the context of a cumulus ensemble model, and the reader is referred to this paper for details of the method. Here we confine ourselves to summarizing the equations for the highly truncated large-scale model assumed by WTG. The domain-averaged potential temperature θ in the cumulus model is assumed to obey

$$\frac{\partial \rho \theta}{\partial t} = \rho (S_\theta - E_\theta) \tag{1}$$

where S_θ is the potential temperature tendency due to radiation, latent heat release, and the vertical eddy transport of heat in the model, averaged over the model domain.[1] The density ρ is assumed to be a function only of height.

The quantity E_θ represents the domain-averaged cooling needed to keep the mean potential temperature profile approximately equal to that of the surrounding environment $\theta_R(z)$. We determine the needed E_θ by a relaxation process dependent on the deviation of the actual mean potential temperature profile $\theta(z)$ from this reference profile:

$$E_\theta = \lambda_x \sin(\pi z/h)[\theta(z) - \theta_R(z)] \tag{2}$$

[1]Note that the notation differs slightly from that of Raymond and Zeng (2005).

for $0 < z < h$, where h is the depth of the troposphere and λ_x is an assumed relaxation rate. The sine function is included in order to make the relaxation strongest in the middle troposphere and zero at the surface and the tropopause. Imagining E_θ to be the consequence of dry adiabatic vertical motions, we define the weak temperature gradient vertical velocity

$$w_D = \frac{E_\theta}{(\partial\theta/\partial z)}, \tag{3}$$

which is simply the domain-averaged vertical velocity needed to produce this adiabatic cooling.

In the boundary layer and near the tropopause (3) provides an unreliable estimate of the vertical velocity, since the potential temperature gradient is small in both regions. For the lowest kilometer, we therefore approximate w_D by a linear interpolation between its value at one kilometer and zero at the surface. For upper levels just below the tropopause where $\partial\theta/\partial z$ is frequently small, we set 1 K km^{-1} as a lower bound for this quantity in (3). Note that the cumulus ensemble model actually has periodic lateral boundary conditions, and hence zero mean vertical velocity, so w_D appears in the model only via the resulting advective tendencies of thermodynamic quantities.

The domain-averaged vertical profile of total cloud water mixing ratio r_t is assumed to obey an equation similar to (1):

$$\frac{\partial \rho r_t}{\partial t} = \rho(S_r - E_r). \tag{4}$$

The quantity S_r is the domain-averaged source of total cloud water and E_r is minus the tendency of cloud water due to environmental motions:

$$E_r = w_D \frac{\partial r_t}{\partial z} + \frac{(r_t - r_x)}{\rho}\frac{\partial \rho w_D}{\partial z}. \tag{5}$$

The first term in this equation represents the effects of large-scale vertical advection, while the second represents entrainment of air from the surrounding environment. Since entrainment occurs when the mass convergence $\partial\rho w_D/\partial z > 0$, we set r_x equal to the reference profile $r_R(z)$ for positive mass convergence and to r_t when mass convergence is negative. This formulation assumes (somewhat unrealistically) that entrained air is immediately mixed in the horizontal through the entire domain. It also neglects the possible effects of ventilation due to a sheared environment. Signs are a bit confusing, since S_r is negative when the modeled convection is removing net water from the column due to precipitation. The quantity $-E_r$ can then be thought of as the rate at which the environment is supplying water vapor to the model domain.

Radiative cooling in this calculation is expressed as a fixed equivalent potential temperature sink set to 2 K d^{-1} up to 12 km, tapering linearly to zero at 15 km.

2.2 Cumulus ensemble model in WTG test cell

The procedure for using these equations is first to create reference profiles of potential temperature $\theta_R(z)$ and total cloud water $r_R(z)$ by integrating the model to a steady equilibrium

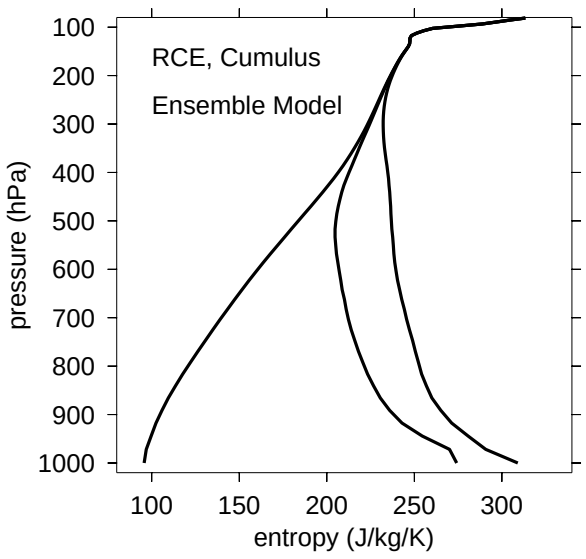

Figure 1: Radiative-convective equilibrium sounding for cumulus ensemble model on 512 km domain. Plotted left to right are curves representing dry entropy, moist entropy, and saturated moist entropy.

state with $\lambda_x = 0$ and with a fixed value of the imposed wind speed and SST. Under these conditions $E_\theta, E_r = 0$, so the equilibrium state is just one of radiative-convective equilibrium in which $S_\theta, S_r = 0$. These equilibrium profiles are then taken as the reference profiles for WTG calculations in which $\lambda_x \neq 0$ and (1) and (4) are integrated to a steady state. Raymond and Zeng (2005) used $\lambda_x = 0.15$ ks^{-1}, or about (2 h)$^{-1}$, and this value is used for all calculations presented in the paper. The WTG calculations are then performed for a variety of imposed wind speeds, and quantities such as equilibrium rainfall rate, evaporation rate, and saturation fraction are computed for each case. Saturation fraction is defined

$$\mathcal{F} = \int_0^\infty \rho r_t dz \Big/ \int_0^\infty \rho r_s dz \tag{6}$$

where r_s is the saturation mixing ratio. The idea is that the resulting values of these quantities should approximate those which would actually occur in the tropical atmosphere for the given surface wind speeds (and hence surface fluxes) and environment defined by the specified reference profiles.

In this paper we adopt the results of Raymond and Zeng (2005) and some additional results for a larger domain as baseline cumulus ensemble calculations. In obtaining these results, the radiative-convective equilibrium calculation assumed an imposed mean surface wind speed of 5 m s^{-1} and an SST of 303 K. The time-averaged domain mean of the latter part of this calculation was used as an environmental reference profile for WTG simulations performed with a variety of imposed wind speeds, but with other parameters the same as in the reference calculation. The results of Raymond and Zeng (2005) were obtained on a two-dimensional domain 50 km in the horizontal and 20 km in the vertical. Subsequently we repeated these calculations with a 512 km horizontal domain, but with no other changes. In both cases the grid size was 500 m in the horizontal by 250 m in the vertical. Figure 1

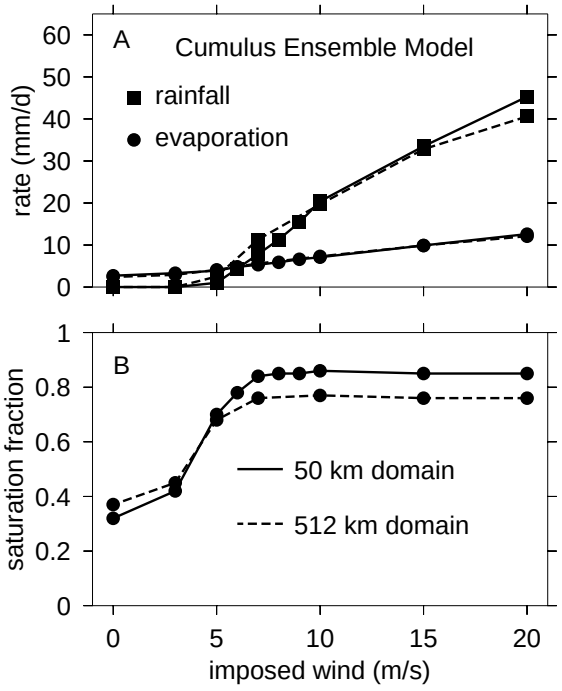

Figure 2: Results of WTG calculations with cumulus ensemble model on 50 km and 512 km domains. (a) Rainfall and evaporation rate in equilibrium as a function of imposed wind speed. (b) Mean equilibrium saturation fraction in model domain as a function of imposed wind speed.

shows the radiative-convective equilibrium sounding for the 512 km domain.

Figure 2 shows how rainfall rate, evaporation rate, and domain-mean saturation fraction vary with imposed wind speed. The results are averages over the last 14 d of 23 d simulations. For low wind speed, rainfall is essentially zero and the saturation fraction is small. As wind speed increases, both the rainfall and the evaporation increase, but the rainfall increases more rapidly, crossing the evaporation curve near a wind speed of 6 m s^{-1}. Saturation fraction asymptotically approaches a limit of about 0.87 for wind speeds in excess of about 7 m s^{-1} for the 50 km domain and about 0.75 for the 512 km domain. Aside from this difference, the curves are remarkably similar for the two domain sizes.

The difference between the rainfall and evaporation rates represents the contribution of moisture convergence to the moisture budget. As the wind speed increases, the ratio of rainfall to evaporation increases, reaching about 3 to 1 at 20 m s^{-1}. Below 6 m s^{-1} moisture divergence occurs since there is less rainfall than evaporation.

As noted in Raymond and Zeng (2005), the rainfall doesn't balance the evaporation at the imposed wind speed 5 m s^{-1}. The imbalance is not large, but there is no reason why it should be exactly zero, as the radiative-convective equilibrium calculation differs slightly from the WTG calculation. In particular, the former lacks the explicit relaxation back toward a reference profile present in the latter.

Table 1: Parameter values in simulations. Other parameters are as listed in table 2. Each test name corresponds to both a set of WTG test cell calculations and a large-scale model integration.

Test	s	λ_p(ks^{-1})	λ_e(ks^{-1})	$\mu(z)$	Comment
OMJO	1	2×10^{-5}	200	shallow	similar to old MJO model
S1	1	1×10^{-4}	300	deep	
S2	2	2×10^{-4}	300	deep	
S4	4	4×10^{-4}	300	deep	best match to cumulus model
S8	8	1×10^{-3}	300	deep	
BISTAB	1	2×10^{-5}	200	deep	bistable for low wind

3 Tuning the cumulus parameterization

In this section we first describe pertinent aspects of the cumulus parameterization. A more complete description is given in the appendix. We then tune the parameterization to mimic the behavior of the cumulus ensemble model using a WTG test cell identical to that used with the cumulus model. The model runs used in this paper are summarized in table 1.

3.1 Convective rain parameterization

The calculations with the cumulus ensemble model are now repeated with a slightly updated version of the toy cumulus parameterization of Raymond and Torres (1998) and Raymond (2000a, 2001). The same fixed radiative cooling and surface flux formulations are used as in the cumulus ensemble model calculations. The bulk of the calculations were made with an SST of 302 K as in Raymond (2001), or 1 K less than for the cumulus ensemble model. Tests at 303 K show no significant differences for the lower SST in the model metrics used in this paper, so comparison with the results of the cumulus ensemble model calculations is justified.

In the present model all precipitation is controlled by the toy cumulus parameterization – there is no "resolved-scale precipitation". Two forms of precipitation are produced by the parameterization, stratiform and convective precipitation. The former simply converts condensate in stratiform cloud regions into precipitation at a rate $\lambda_s = 0.1$ ks^{-1}. The rate limiting process is not this rate, but the rate at which the large-scale model supplies condensate. Thus, there is little to tune in this part of the precipitation parameterization.

In contrast, there are a number of parameters controlling the rate at which convective precipitation is produced, and the behavior of the WTG calculation is sensitive to these parameters. Equation (23) shows that the convective part of precipitation production takes the form

$$C_{Rc} = \lambda_p (r_v/r_s)^s \mu(z) \tag{7}$$

where r_v is the vapor mixing ratio, r_s is the saturation mixing ratio, $\mu(z)$ is a shape function, and λ_p and s are constants. The parameter s is the "stiffness", or the sensitivity of convective precipitation production to changes in relative humidity r_v/r_s; it and the convective precipitation rate constant λ_p turn out to play a crucial role when the parameterization is embedded in a large-scale dynamical model.

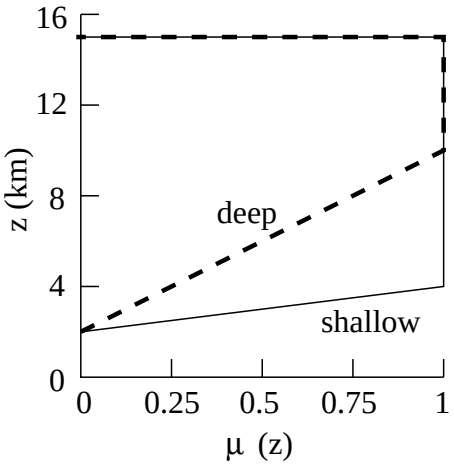

Figure 3: Shallow (solid) and deep (dashed) forms of the convective precipitation shape function $\mu(z)$ employed in this paper.

This form of convective precipitation production is subject to numerical problems in the upper troposphere, where the conversion of vapor to precipitation in one time step can easily exceed the mixing ratio of vapor at that level. This problem is solved by limiting the rate predicted by (7) at each level to 30% per kilosecond of the available vapor at that level. Since all time steps used in this paper are less than 1 ks, numerical difficulties are avoided.

The two forms of the shape function $\mu(z)$ used in this paper are illustrated in figure 3. In both cases convective precipitation conversion begins at $z = 2$ km and ends at the top of the convection. In the "shallow" case, conversion reaches full strength at $z = 4$ km whereas this is delayed until 10 km in the "deep" case. In terms of the model parameters, the shallow case corresponds to $z_p = 3$ km and $z_s = 2$ km, whereas in the deep case, $z_p = 6$ km and $z_s = 8$ km. The form of $\mu(z)$ has a strong effect on the radiative-convective equilibrium potential temperature (or dry entropy) profile.

3.2 Cumulus parameterization in WTG test cell

The first calculation in this subsection employs parameters which approximate those used in the MJO simulations of Raymond (2001), i. e., with $s = 1$, $\lambda_p = 2\times10^{-5}$ ks^{-1}, $\lambda_e = 200$ ks^{-1}, and a shallow convective precipitation profile, but with cloud-radiation interactions turned off (test OMJO in table 1). Figure 4 shows that the rainfall rate does not increase nearly as much with wind speed as it does in the cumulus ensemble model results shown in figure 2. At a wind speed of 20 m s^{-1}, the rainfall rate is only twice the evaporation rate, whereas it is three times the evaporation rate at this wind speed for the cumulus ensemble model. This ratio is of fundamental importance, because it expresses the amount of latent heat release produced, and hence the strength of the resulting thermal circulations, in response to a given surface evaporation rate.

As figure 5 shows, the radiative-convective equilibrium state produced by the parameterization with this set of precipitation parameters is considerably more moist than in the cumulus ensemble results (compare with figure 1). Increasing the convective precipitation

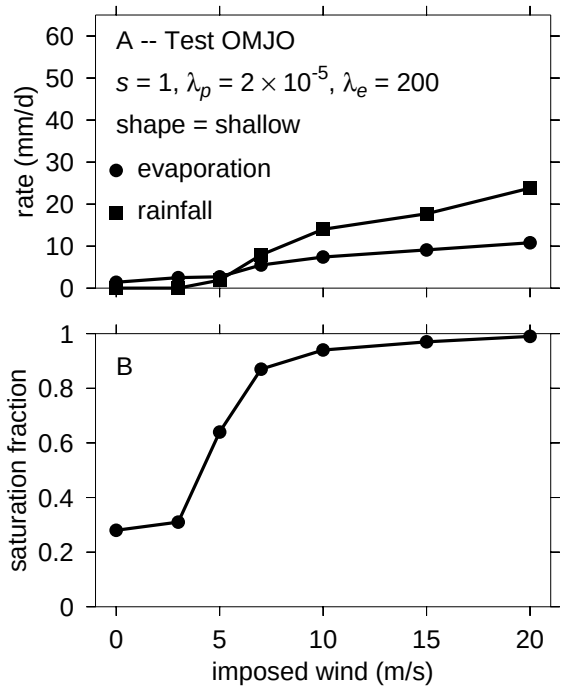

Figure 4: Results of WTG calculations using the cumulus parameterization with parameters characteristic of the MJO simulations by Raymond (2001; test OMJO). Otherwise, like figure 2.

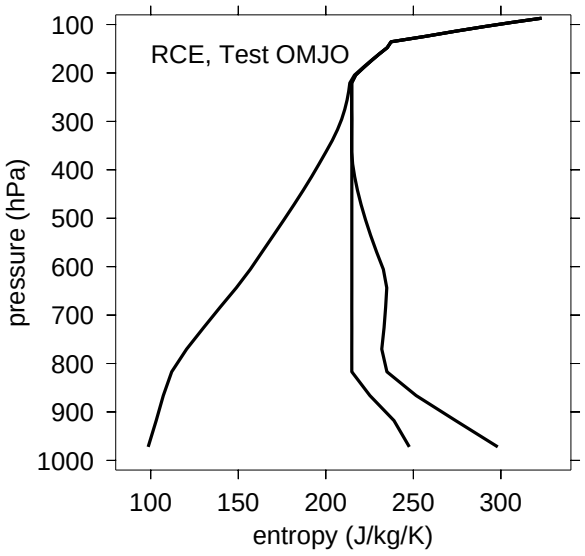

Figure 5: Radiative-convective equilibrium profiles from the cumulus parameterization of (left to right) dry entropy, moist entropy, and saturated moist entropy for the case of figure 4.

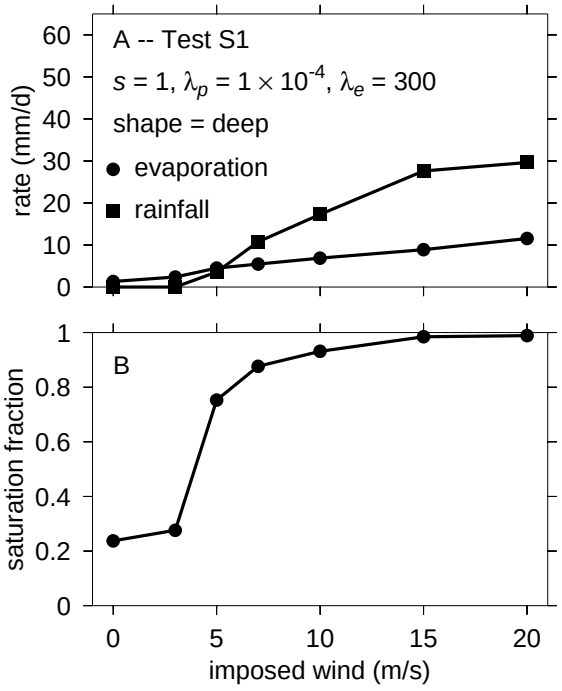

Figure 6: As in figure 4 except with test S1.

rate λ_p decreases the upper tropospheric humidity in the model, but by itself increases the dry static stability to unacceptable levels in the lower troposphere. However, changing to the deep convective precipitation profile alleviates this problem.

Figure 6 shows the rainfall and evaporation rates as well as the saturation fraction as a function of imposed wind speed for parameter values $s = 1$, $\lambda_p = 1 \times 10^{-4}$ ks^{-1}, $\lambda_e = 300$ ks^{-1}, and for a deep convective precipitation profile (test S1 in table 1), while figure 7 shows the corresponding radiative-convective equilibrium sounding. The profiles of moist entropy and saturated moist entropy are significantly different than those produced by the cumulus ensemble model. However, the relative humidity as a function of height (as indicated by the value of the moist entropy relative to the dry and saturated moist entropies at each height) approximates that produced by the cumulus ensemble model. Increasing the value of λ_p by a factor of 5 over that in the previous case thus has the desired effect in this regard. However, as figure 6 shows, the increase in rainfall rate with imposed wind speed still does not match the cumulus ensemble model results, though it is an improvement over the previous case.

Three additional WTG runs were made with increasing values of stiffness s, listed as tests S2, S4, and S8 in table 1. As s was increased, λ_p had to be increased also, as shown in this table, in order to maintain a realistic relative humidity profile. Figure 8 shows the rainfall rate, etc., as a function of imposed wind speed for the case (test S4) with $s = 4$ and $\lambda_p = 4 \times 10^{-4}$ ks^{-1}. This case produced results closer to the cumulus ensemble results than any of the others. In particular, the precipitation rate as a function of wind speed matches the cumulus model reasonably well. The saturation fraction as a function of imposed wind speed shows general agreement but significant differences in detail. Given the simple nature

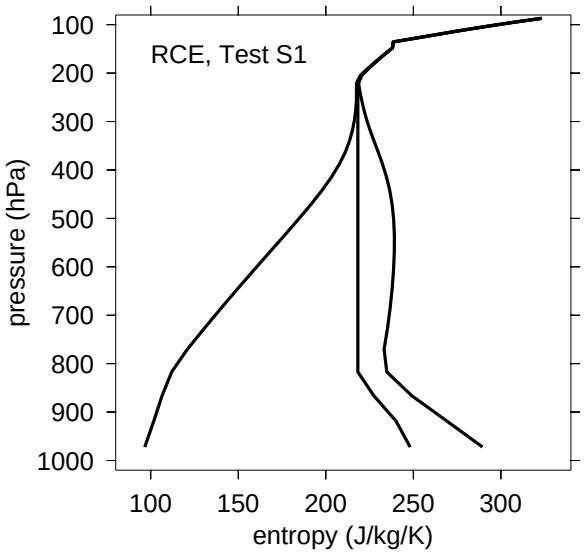

Figure 7: As in figure 5 except for test S1.

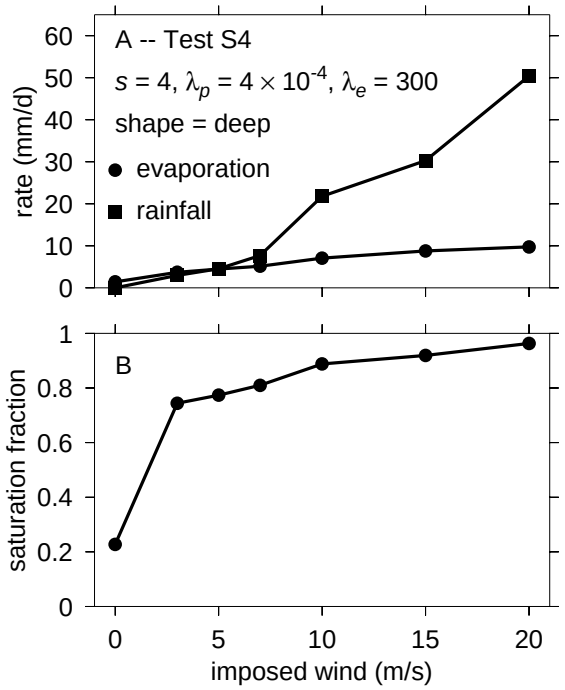

Figure 8: As in figure 4 except for test S4.

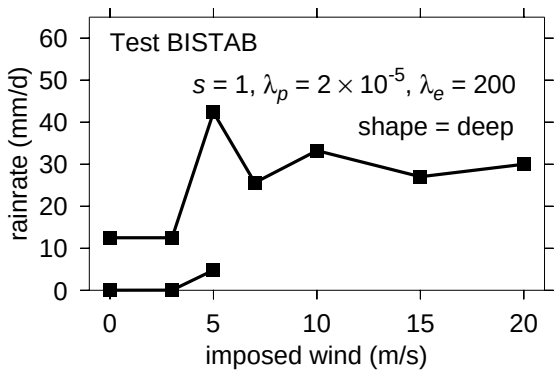

Figure 9: Rainfall rate as a function of imposed wind speed for test BISTAB. In this test two different equilibrium rainfall rates exist for low wind speeds.

of the cumulus parameterization, the agreement is reasonable.

Interesting behavior occurs when the OMJO WTG test cell calculation is altered solely by changing the convective precipitation profile from shallow to deep. This simulation exhibits bistable behavior for wind speeds ≤ 5 m s^{-1}, with two possible equilibrium values of rainfall rate. This behavior is illustrated in figure 9 and the simulation is labeled BISTAB in table 1. Such behavior is reminiscent of that noted in the two-column simulations of Raymond and Zeng (2000) using an earlier version of the cumulus parameterization employed here. In light of these earlier results, the cumulus ensemble model was tested carefully, and such bistable behavior was not found. Thus, if the cumulus ensemble model is representative of the real world, such bistable behavior in the earlier two-column model, and in the current WTG model with this choice of parameters, must be spurious.

Note that two types of bistability were found by Raymond and Zeng (2000), that occurring with and without cloud-radiation interactions. Since the cumulus ensemble model calculations of Raymond and Zeng (2005) were done with fixed radiative cooling, we can draw no conclusions as to whether radiative effects can induce bistable behavior in the real world.

4 Large-scale simulations

In this section we investigate the sensitivity of large-scale model simulations to the above-described changes in the cumulus parameterization. A series of aquaplanet channel model simulations on an equatorial beta plane was run using a slightly improved version of the model of Raymond (2001). The main difference is that the model is recoded in the C language. Other differences are in the numerics and in the cumulus parameterization. Unlike the earlier model, all variables are cell-centered. Weak ∇^4 smoothing reduces the need for other forms of damping, resulting in a more lively model. The cumulus parameterization used is described in this paper. Tuning the cumulus parameterization to the cumulus ensemble model results in significant changes in the large-scale circulations predicted by this model.

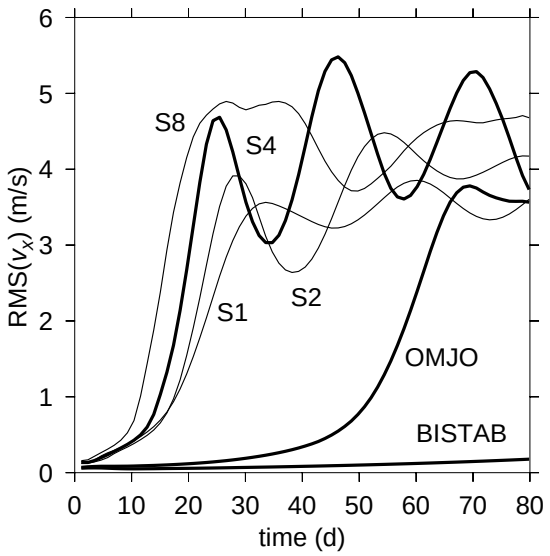

Figure 10: Root-mean-square variance as a function of time of surface zonal wind within 3000 km of the equator for the cases listed in table 1.

4.1 Initiation of simulations

The computational domain is 40000 km in x (east) by 10000 km in y (north), centered on the equator, and with a horizontal cell size of $\Delta x = \Delta y = 250$ km. The domain top is 80 hPa with an assumed domain-top potential temperature of 380 K. Forty vertical levels are used, so that $\Delta\sigma = 0.025$. All variables are defined on cell centers. Simulations are started from rest with a constant SST of 302 K and a profile of temperature and humidity obtained from a radiative-convective equilibrium calculation run with an assumed surface wind of 5 m s^{-1}. The same cloud physics parameters are used in the simulation and the radiative-convective equilibrium calculation in each case. A noise pattern is applied initially to the lower troposphere humidity field of the form

$$r_t \leftarrow r_t[1 + 0.3\mathcal{R}(z/z_s)\exp(1 - z/z_s)] \tag{8}$$

where $z_s = 3$ km and where for each grid point $\mathcal{R}$ varies randomly over the interval $[-1, 1]$. The calculations are then run for 20000 ks, or about 231 d. Any disturbances grow out of this noise field. Note that unlike Raymond (2000a, 2001), cloud-radiation interactions are turned off for these simulations.

4.2 Simulation results

For each of the WTG test cell cases presented in section 3, corresponding equatorial beta plane simulations were made with identical precipitation parameters. These cases are listed in table 1. In all cases growing disturbances develop out of the random humidity noise. However, the rate of development varies significantly from case to case. Details of these simulations are not presented; only their gross statistical characteristics are discussed here.

Figure 10 shows that the cases with the largest values of the precipitation stiffness parameter s develop the most rapidly. Among those cases with the same stiffness $s = 1$ (OMJO,

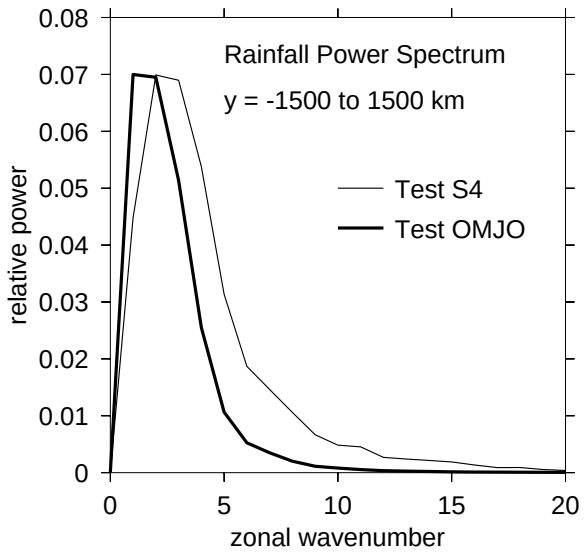

Figure 11: Zonal power spectrum of rainfall rate for cases OMJO and S4, averaged in time over the last half of the simulation and in latitude over the interval -1500 km $\leq y \leq$ 1500 km. The zonal wavenumber is the x domain size of 40000 km divided by the wavelength.

S1, BISTAB), shallow as opposed to deep convective precipitation profiles and larger values of the precipitation conversion rate λ_p favor more rapid growth. The BISTAB case hardly develops at all in the period shown.

In terms of observable output rather than model parameters, examination of figures 4, 6, 8, and 9 shows that the steeper the dependence of equilibrium rainfall rate on imposed wind speed, the more rapidly the disturbance develops. Thus, the sensitivity of the equilibrium rainfall rate to surface wind speed, and hence the total surface heat flux, appears to be a good indicator of the rate of development of large-scale tropical disturbances in the present model. The significance of this discovery is discussed later.

A zonal power spectral analysis of the variance of rainfall rate averaged over -1500 km $\leq y \leq 1500$ km and the last half of the simulation is shown for the cases OMJO and S4 in figure 11. Comparing the two, the peak in the variance is shifted from zonal wavenumber 1 to 2 in S4, and much more variance exists at shorter wavelengths. This emphasizes how important the change in the cumulus parameterization is for the development of disturbances on the scale of a few thousand kilometers.

Figure 12 is a combined zonal-time power spectral analysis for cases OMJO and S4 similar to that performed by Wheeler and Kiladis (1999), except that the red noise background is not subtracted and both equatorially symmetric and antisymmetric disturbances are included. The increase in power at higher wavenumbers is seen as in figure 11. In OMJO the only deviation from red noise is the tendency of disturbances to move to the west, as indicated by the concentration of power at negative wavenumbers. This slow westward drift may be simply the result of westward advection with the easterly trade winds. A tendency toward westward drift is evident in the S4 case as well, but eastward propagation is also present, as indicated by the spectral power at large frequency and positive wavenumber. Some hint of Kelvin and Madden-Julian modes is thus present at low amplitude, though the spectral

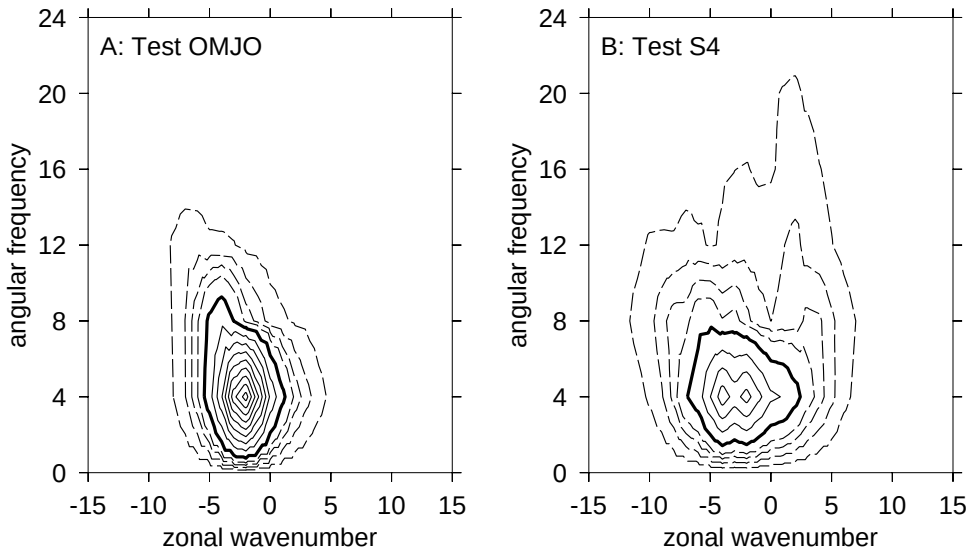

Figure 12: Joint zonal-time power spectrum of rainfall for (a) test OMJO and (b) test S4. Solid contours start at 60 (heavy line), incrementing by 60. Dashed contours start at 10, incrementing by 10 up to 40. Power units are arbitrary. The zonal wavenumber k, the latitudinal averaging, and the analyzed time interval are as in figure 11 and ω is scaled so that the phase speed ω/k has the units of meters per second. The rainfall is de-trended in time before the spectrum is computed and the spectrum is smoothed slightly in wavenumber.

distribution is still quite different from that observed in the earth's atmosphere. However the sea surface temperature is uniform, and thus not representative of the actual distribution. Imposition of a realistic distribution results in much stronger eastward propagation (results not shown). Since the focus of this paper is on more general questions, the behavior of the model with realistic boundary conditions is not pursued further here.

5 Discussion and conclusions

This paper presents two main results, one specific and one general. The general result is a demonstration of how a cumulus ensemble model run in weak temperature gradient mode can be used to test a cumulus parameterization. We note that the testing presented here is only for the equilibrium behavior of convection. Tests of transient behavior remain to be implemented. This could be done, for instance, by imposing a reference profile which is an oscillatory function of time.

The specific result is that we have exposed an important sensitivity in cumulus parameterizations – the rate of increase of equilibrium precipitation rate with surface wind speed. Two parameters in the cumulus parameterization are responsible for most of the changes in model behavior: one, λ_p, controls the conversion rate of water vapor to precipitation at a specific environmental relative humidity and the other, s, controls how rapidly the precipitation rate increases as relative humidity increases. We now examine the significance of these parameters.

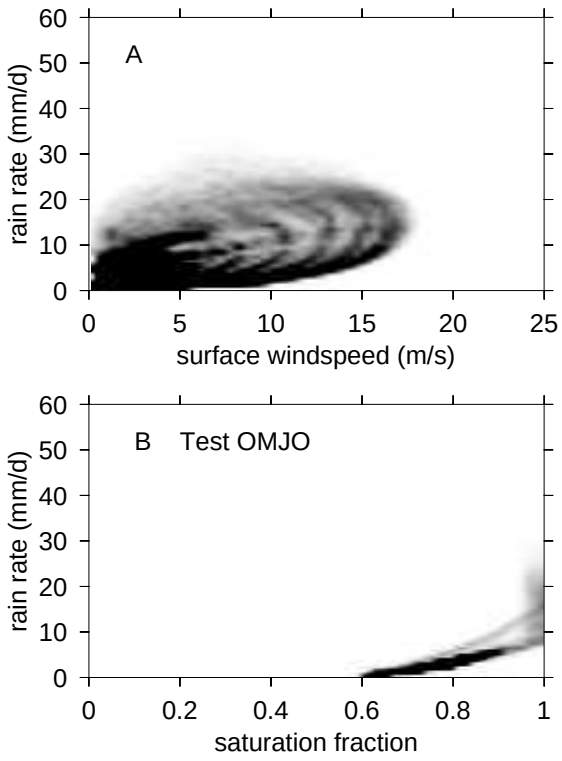

Figure 13: Joint frequency distributions between (a) rainfall rate and surface wind speed and (b) rainfall rate and saturation fraction for test OMJO. Sample is limited to within 2000 km of the equator and the last half of the simulation. The darker the gray scale, the higher the frequency of occurrence.

Fuchs and Raymond (2002, 2005) developed a linearized model of the large-scale tropical flow, based on a highly simplified treatment of rainfall, which assumes that the deviation of the precipitation rate from that in a radiative-convective equilibrium state takes the form

$$P' = \alpha Q', \tag{9}$$

where Q' is the deviation in the precipitable water from the radiative-convective equilibrium value and α is a rate constant.[2] The corresponding relation in the present model may be written approximately as

$$P = P_R (Q/Q_R)^s, \tag{10}$$

where s is the stiffness parameter discussed earlier, and where λ_p is incorporated into the radiative-convective equilibrium values of precipitation rate P_R and precipitable water Q_R. Identifying $P' = P - P_R$ and $Q' = Q - Q_R$, (10) may be linearized as

$$P' = s(P_R/Q_R)Q'. \tag{11}$$

[2]An additional term in this equation involving the deviation in the convective available potential energy from its equilibrium value is omitted here for simplicity.

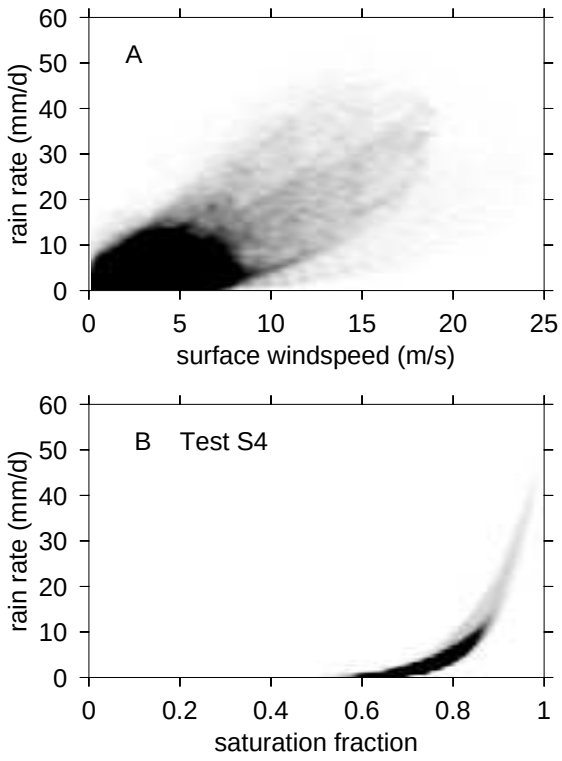

Figure 14: As in figure 13 except for test S4.

Comparison with (9) shows that the moisture equilibration rate constant α is given by

$$\alpha = s(P_R/Q_R). \tag{12}$$

For typical tropical equilibrium values $P_R = 4$ mm d^{-1}, $Q_R = 50$ mm, and $(P_R/Q_R)^{-1} \approx 12$ d. Thus, if $s = 1$, then $\alpha^{-1} \approx 12$ d, which is much longer than the value 1 d chosen by Fuchs and Raymond (2005) or the value range $0.5 - 2.5$ d found by Sobel and Bretherton (2003) and Bretherton et al. (2004) from numerical modeling and observation. Our favored value $s = 4$ yields $\alpha^{-1} \approx 3$ d, which is much closer to the above range. Thus, our cumulus ensemble model and the results of Sobel and Bretherton (2003) on one hand and Bretherton et al. (2004) on the other are in agreement within a factor of two. Our work suggests that α^{-1} is a factor of four smaller than the natural moisture adjustment time scale Q_R/P_R due to the stiffness of the humidity-precipitation rate relationship.

These results indicate that the time scales for moisture adjustment computed in the simple schematic model of Raymond (2000b) are too long due to the simple inverse relationship between saturation deficit and precipitation rate assumed in that paper. A stiffer dependence of rainfall on saturation deficit would reduce adjustment time scales in that model as well.

Figures 13 and 14 show joint frequency distributions for tests OMJO and S4 between rainfall rate and surface wind speed on one hand and rainfall rate and saturation fraction on the other. The tight relationship between rainfall rate and saturation fraction seen in the WTG simulations is maintained in the beta plane model runs. However, this relationship is much more like that observed in the cumulus ensemble model results in S4 than it is in

OMJO. In the latter case near-saturation of the troposphere was needed to produce heavy rainfall. The modified treatment of convective rainfall has changed this picture completely in S4. The sort of relationship between rainfall rate and saturation fraction seen in S4 is found in the real world according to the observations of Bretherton et al. (2004).

In a steady state the present model yields a one-to-one relationship between surface wind speed and rainfall rate as well as between saturation fraction and rainfall. As figures 13 and 14 show, this relationship exists also in the beta plane model result, but is much less sharp than for saturation fraction and rainfall. This means that the equilibration time for the vertical rearrangement of moisture by convection is much smaller than the time scale for changing the total amount of moisture in a column. Evidently the convection itself effects this redistribution very rapidly, at least in the cumulus ensemble model and in the cumulus parameterization, resulting in the well-defined precipitation-saturation fraction results seen. In short, it appears that the equilibrium time for vertical redistribution of moisture is less than the dynamical time scale of the modeled disturbances, while the equilibrium time for the lateral distribution of moisture is longer than the dynamical time scale.

As Derbyshire et al. (2004) noted, many cumulus parameterizations do not reproduce the strong sensitivity of precipitation to tropospheric humidity. The present results show that this sensitivity has significant dynamical consequences. In particular, increased sensitivity of this type results in more rainfall variance at smaller space and time scales.

The role of cloud-radiation interactions in destabilizing intraseasonal disturbances is a confusing and controversial issue at this point, and the fact that the model of Raymond (2001) and the current, nearly identical model cannot agree on this question illustrates how sensitive these disturbances are to small changes. However, the present result that cloud-radiation interactions are not needed to destabilize the environment is in agreement with Grabowski (2003) and Grabowski and Moncrieff (2004).

Acknowledgments. Thanks go to Adam Sobel and Chris Bretherton for extensive discussions about the weak temperature gradient approximation. This work was supported by National Science Foundation Grant No. 0352639.

6 Appendix: The cumulus parameterization

The cumulus parameterization is descended from that of Raymond and Torres (1998) and Raymond (2000a, 2001). It is an adjustment scheme, with separate calculations made for shallow and deep convection. The forms of the convective source terms for each type of convection are similar; for equivalent potential temperature θ_e, total cloud water mixing ratio r_t, and the horizontal velocity $\mathbf{v}$, they are

$$S_{eci} = \left(\overline{\theta}_e - \theta_e(z) + \frac{F_e}{M} \right) \eta(z) \tag{13}$$

$$S_{ri} = \left(\overline{r}_t - r_t(z) + \frac{F_r}{M} \right) \eta(z) - C_R(z) \tag{14}$$

$$\mathbf{S}_{vi} = \left(\overline{\mathbf{v}} - \mathbf{v}(z) + \frac{\mathbf{F}_v}{M} \right) \eta(z) \tag{15}$$

where F_e, F_r, and $\mathbf{F}_v$ are the surface fluxes of the corresponding variables, M is the mass per unit area in the column extending from the surface to the top of the convection, and $\eta(z)$ is the rate function

$$\eta(z) = \lambda_c(1 + az/d)\Lambda(d - z) \tag{16}$$

where d is the depth of the convective layer, a and λ_c are constants, and with $\Lambda(x) = 1$ for $x > 0$ and $\Lambda(x) = 0$ for $x < 0$.

Separate calculations are made for shallow and deep convection. Shallow, planetary boundary layer (PBL) convection is assumed to have the prescribed depth $d = b$. The depth $d = D$ of deep convection is assumed to be the level of neutral buoyancy for parcels with average characteristics of the PBL, i. e., averaged over the height range $0 < z < b$. In calculating this, the highest level of neutral buoyancy is taken, thus ignoring possible inversions and stable layers at intermediate altitudes. The value $a = 0$ is used in (16) for deep convection, while $a = -1$ is used for shallow convection.

Observations over warm tropical oceans generally show positive buoyancy for PBL parcels everywhere in the troposphere except for a stable layer just above the PBL (Raymond et al., 2003). The partitioning between shallow and deep convection in each grid box is decided on the basis of the convective inhibition in this layer. The parameter ϵ is taken as a measure of this inhibition:

$$\epsilon = \mathcal{T}(\theta_{eb} - \theta_{et}, \Delta\theta_e), \tag{17}$$

where $\Delta\theta_e$ is a constant, θ_{eb} is the mean equivalent potential temperature in the height range $0 < z < b$ and θ_{et} is the mean saturated equivalent potential temperature in the range $b < z < 2b$. The function $\mathcal{T}(x, y)$ is a "throttle function", i. e.,

$$\mathcal{T}(x,y) = \begin{cases} 0, & x < -y/2 \\ x/y + 1/2, & -y/2 < x < y/2 \\ 1, & x > y/2 \end{cases} . \tag{18}$$

Actual profiles of convective source terms are computed as weighted averages of the shallow and deep convective profiles, indicated respectively by subscripted s and d:

$$S_{ec} = \epsilon S_{ecd} + (1 - \epsilon)S_{ecs} \tag{19}$$

etc.

The overbar applied to any variable $\chi(z)$ is

$$\overline{\chi} = \frac{1}{M}\int_0^d \rho(z)\eta(z)\chi(z)dz \tag{20}$$

where $\rho(z)$ is the atmospheric density profile and where

$$M = \int_0^d \rho(z)\eta(z)dz. \tag{21}$$

Equations (13)-(15) are designed so that, for instance,

$$\int_0^d \rho(z)[\overline{\theta}_e - \theta_e(z)]\eta(z)dz = 0. \tag{22}$$

Thus, the first two terms represent a conservative redistribution or adjustment which attempts to homogenize vertically the variable in question. The third term on the right of these equations represents the vertical distribution of surface fluxes. This distribution is weighted by the function $\eta(z)$.

The vertical profile $C_R(z)$ represents the conversion of total cloud water (vapor plus cloud droplets) to precipitation, and it takes a rather complex form

$$\begin{aligned} C_R &= \lambda_p(r_v/r_s)^s\mu(z) + \lambda_s(r_t - r_s)\Lambda(r_t - r_s)\mathcal{T}(\Gamma_e - \Gamma_t, \Gamma_s) \\ &\quad -\lambda_e(r_s - r_t)\Lambda(r_s - r_t)r_p \end{aligned} \tag{23}$$

involving three terms.

The third term represents the evaporation of precipitation. The quantities r_s and r_p are the saturation and precipitation mixing ratios and λ_e is a constant controlling the evaporation rate.

The second term represents the formation of precipitation in regions that are saturated on the large scale, and λ_s is the rate constant controlling this process. The quantity $\Gamma_e = d\theta_e/dz$ and Γ_t is a constant threshold value of Γ_e, while Γ_s defines the range over which the throttle function turns on. The purpose of the throttle function in the second term of (23) is to suppress the conversion of cloud water to precipitation in saturated regions where $\Gamma_e < 0$. Since grid-scale saturation with negative Γ_e is unstable, it cannot exist for long. Such regions are viewed as being mainly unsaturated, but pierced by saturated columns of convection of sufficient density to render the average cloud water content saturated. The instability in this case resides solely in the convective columns, and it is inappropriate to turn on "stratiform" processes there.

The first term represents the conversion of cloud water to precipitation by convective columns in regions which may or may not be saturated on the grid scale. This process is governed by the rate constant λ_p and is assumed to be proportional to the relative humidity r_v/r_s to the power s, which is called the stiffness of the dependence of precipitation on relative humidity. The variable r_v is the water vapor mixing ratio. The function $\mu(z)$ takes the assumed form

$$\mu(z) = \mathcal{T}(z - z_p, z_s)\Lambda(d - z). \tag{24}$$

It thus causes convective precipitation formation to turn on starting at height $z = z_p - z_s/2$, with full strength reached at height $z = z_p + z_s/2$. In any case, convective precipitation is not allowed above the convective top $z = d$. The reasoning here is that shallow clouds do not precipitate. In addition, if the convective precipitation term as calculated above removes more than 30% of r_t in a single time step, it is limited to this 30% magnitude, thus suppressing unphysical oscillations in the simulation.

The vertical profile of precipitation rate $P = \rho w_t r_p$ is assumed to adjust instantly to conditions in the grid box, and thus obeys the time-independent vertical advection equation

$$\frac{1}{\rho}\frac{\partial P}{\partial z} = -C_R, \tag{25}$$

with $P = 0$ at the top of the domain. Thus, integrating (25) down from the top yields the precipitation rate at the surface.

Table 2: Parameters used in the cumulus parameterization.

Parameter	Value	Meaning
λ_c	0.003 ks^{-1}	convective mixing
λ_p	various (ks^{-1})	convective precipitation
λ_s	0.1 ks^{-1}	stratiform precipitation
Γ_t, Γ_s	2 K km^{-1}(both)	lower bound of $d\theta_e/dz$ for strat precip
λ_e	various (ks^{-1})	evaporation of rain
s	various (dimensionless)	convective rain production stiffness
z_p, z_s	various (km)	convective rain height distribution
w_t	5 m s^{-1}	precipitation terminal velocity
b	1.5 km	depth of PBL
$\Delta\theta_e$	4 K	slop in convective throttle
ΔT	0.5 K	slop in surface flux throttle
C_D	0.001	surface drag coefficient
W	3 m s^{-1}	minimum wind for surface fluxes

A simplified definition of equivalent potential temperature is used in this parameterization:

$$\theta_e = \theta \exp(\gamma r_t), \tag{26}$$

where $\gamma = L/(C_p T_R)$, $L = L_c + L_f$ is the sum of the latent heats of condensation and freezing, C_p the specific heat of air at constant temperature, and $T_R = 300$ K a constant reference temperature. The total cloud water mixing ratio r_t is used instead of the vapor mixing ratio, because the difference between the two is likely to be small when averaged over grid boxes typical of large-scale models.

The potential temperature source term is computed from the equivalent potential temperature and total water source terms using

$$S_\theta = \theta[(S_{ec} + S_{er})/\theta_e - \gamma S_r] \tag{27}$$

where S_{ec} and S_{er} are the convective and radiative contributions to the equivalent potential temperature source, S_r is the convective source of total water mixing ratio, and γ is defined above. The total precipitation rate is the weighted average of the contributions from shallow and deep convection:

$$P = \epsilon P_d + (1 - \epsilon) P_s. \tag{28}$$

Surface fluxes for each intensive variable χ are calculated using a simple bulk formula:

$$F_\chi = \mathcal{T}(T_{ss} - T_b, \Delta T)\rho_b C_D(|\mathbf{v}_b|^2 + W^2)^{1/2}(\chi_{ss} - \chi_b) \tag{29}$$

where T_{ss} is the temperature of the sea surface, T_b is the temperature of the air in the boundary layer adjacent to the surface, ΔT and W are a constants, C_D is the (constant) drag coefficient, a subscripted b indicates a boundary layer value, and a subscripted ss indicates a sea surface value. The throttle function turns the fluxes off when $T_b > T_{ss} + \Delta T/2$.

Table 2 lists values of parameters used in the cumulus and surface flux parameterizations. The radiation parameterization is that presented in Raymond and Torres (1998) and Raymond (2000a, 2001).

7 References

Bergman, J. W., and P. D. Sardeshmukh, 2004: Dynamic stabilization of atmospheric single column models. *J. Climate,* **17,** 1004-1021.

Bretherton, C. S., M. E. Peters, and L. E. Back, 2004: Relationships between water vapor path and precipitation over the tropical oceans. *J. Climate,* **17,** 1517-1528.

Derbyshire, S. H., I. Beau, P. Bechtold, J.-Y. Grandpeix, J.-M. Piriou, J.-L. Redelsperger, and P. M. M. Soares, 2004: Sensitivity of moist convection to environmental humidity. *Quart. J. Roy. Meteor. Soc.,* **130,** 3055-3079.

Fuchs, Ž., and D. J. Raymond, 2002: Large-scale modes of a nonrotating atmosphere with water vapor and cloud-radiation feedbacks. *J. Atmos. Sci.,* **59,** 1669-1679.

Fuchs, Ž., and D. J. Raymond, 2005: Large-scale modes in a rotating atmosphere with radiative-convective instability and WISHE. *J. Atmos. Sci.,* **62,** 4084-4094.

Grabowski, W. W., 2001: Coupling cloud processes with the large-scale dynamics using the cloud-resolving convection parameterization (CRCP). *J. Atmos. Sci.,* **58,** 978-997.

Grabowski, W. W., 2003: MJO-like coherent structures: Sensitivity simulations using the cloud-resolving convection parameterization (CRCP). *J. Atmos. Sci.*, **60**, 847-864.

Grabowski, W. W., and M. W. Moncrieff, 2004: Moisture-convection feedback in the tropics. *Quart J. Roy. Meteor. Soc.*, **130**, 3081-3104.

Grabowski, W. W., and P. K. Smolarkiewicz, 1999: CRCP: A cloud resolving convection parameterization for modeling the tropical convecting atmosphere. *Physica D*, **133**, 171-178.

Grabowski, W. W., X. Wu, and M. W. Moncrieff, 1996: Cloud-resolving modeling of tropical cloud systems during phase III of GATE. Part I: Two-dimensional experiments. *J. Atmos. Sci.,* **53,** 3684-3709.

Khairoutdinov, M. F., and D. A. Randall, 2001: A cloud-resolving model as a cloud parameterization in the NCAR Community Climate System Model: Preliminary results. *Geophys. Res. Letters*, 28, 3617-3620.

Maloney, E. D., and D. L. Hartmann, 2001: The sensitivity of intraseasonal variability in the NCAR CCM3 to changes in convective parameterization. *J. Climate,* **14,** 2015-2034.

Mapes, B. E., 2004: Sensitivities of cumulus-ensemble rainfall in a cloud-resolving model with parameterized large-scale dynamics. *J. Atmos. Sci.*, **61**, 2308-2317.

Mapes, B. E., T. T. Warner, M. Xu, and D. J. Gochis, 2004: Comparison of cumulus parameterizations and entrainment using domain-mean wind divergence in a regional model. *J. Atmos. Sci.,* **61,** 1284-1295.

Randall, D., M. Khairoutdinov, A. Arakawa, and W. Grabowski, 2003: Breaking the cloud parameterization deadlock. *Bull. Am. Meteor. Soc.,* **84,** 1547-1564.

Randall, D. A., K.-M. Xu, R. J. C. Somerville, and S. Iacobellis, 1996: Single-column models and cloud ensemble models as links between observations and climate models. *J. Climate,* **9,** 1683-1697.

Raymond, D. J., 2000a: The Hadley circulation as a radiative-convective instability. *J. Atmos. Sci.,* **57,** 1286-1297.

Raymond, D. J., 2000b: Thermodynamic control of tropical rainfall. *Quart. J. Roy. Meteor. Soc.,* **126,** 889-898.

Raymond, D. J., 2001: A new model of the Madden-Julian oscillation. *J. Atmos. Sci.,* **58,** 2807-2819.

Raymond, D. J., G. B. Raga, C. S. Bretherton, J. Molinari, C. Lopez-Carrillo, and Z. Fuchs, 2003: Convective forcing in the intertropical convergence zone of the eastern Pacific. *J. Atmos. Sci.,* **60,** 2064-2082.

Raymond, D. J., and D. J. Torres, 1998: Fundamental moist modes of the equatorial troposphere. *J. Atmos. Sci.,* **55,** 1771-1790.

Raymond, D. J., and X. Zeng, 2000: Instability and large-scale circulations in a two-column model of the tropical troposphere. *Quart. J. Roy. Meteor. Soc.,* **126,** 3117-3135.

Raymond, D. J., and X. Zeng, 2005: Modelling tropical atmospheric convection in the context of the weak temperature gradient approximation. *Quart. J. Roy. Meteor. Soc.,* **131,** 1301-1320.

Slingo, J., M. Blackburn, A. Betts, R. Brugge, K. Hodges, B. Hoskins, M. Miller, L. Steenman-Clark, and J. Thuburn, 1994: Mean climate and transience in the tropics of the UGAMP GCM: Sensitivity to convection parameterization. *Quart. J. Roy. Meteor. Soc.,* **120,** 881-922.

Sobel, A. H., and C. S. Bretherton, 2000: Modeling tropical precipitation in a single column. *J. Climate,* **13,** 4378-4392.

Sobel, A. H., and C. S. Bretherton, 2003: Large-scale waves interacting with deep convection. *Tellus,* **55a**, 45-60.

Sobel, A. H., J. Nilsson, and L. M. Polvani, 2001: The weak temperature gradient approximation and balanced tropical moisture waves. *J. Atmos. Sci.*, **58**, 3650-3665.

Wang, W.-Q., and M. E. Schlesinger, 1999: The dependence on convection parameterization of the tropical intraseasonal oscillation simulated by the UIUC 11-layer atmospheric GCM. *J. Climate,* **12,** 1423-1457.

Wheeler, M., and G. N. Kiladis, 1999: Convectively coupled equatorial waves: Analysis of clouds and temperature in the wavenumber-frequency domain. *J. Atmos. Sci.*, **56**, 374-399.

Xu, K.-M., and D. A. Randall, 1996: Explicit simulation of cumulus ensembles with the GATE phase III data: Comparison with observations. *J. Atmos. Sci.,* **53,** 3710-3736.

Zhang, C., M. Dong, S. Gualdi, H. H. Hendon, E. D. Maloney, A. Marshall, K. R. Sperber, and W. Wang, 2006: Simulations of the Madden-Julian oscillation in four pairs of coupled and uncoupled global models. *Climate Dynamics*, DOI 10.1007/s00382-006-0148-2.

Zhang, G. J., and M. Q. Mu, 2005: Simulation of the Madden-Julian oscillation in the NCAR CCM3 using a revised Zhang-McFarlane convection parameterization scheme. *J. Climate,* **18,** 4046-4064.